Acta Pharmaceutica Sinica B 2026;16(5):3074−3089

Chinese Pharmaceutical Association
Institute of Materia Medica, Chinese Academy of Medical Sciences

Acta Pharmaceutica Sinica B

www.elsevier.com/locate/apsb
www.sciencedirect.com

ORIGINAL ARTICLE

Targeting cancer-associated fibroblast-activated HGF/c-MET pathway inhibits extrahepatic cholangiocarcinoma progression and restores gemcitabine therapeutic sensitivity

Mingzhen Bai[a,b,c,†], Ping Yue[a,†], Wenkang Fu[a,†], Ruyang Zhong[a,†], Chongfei Huang[a], Ningzu Jiang[a], Long Gao[a], Ningning Mi[a], Haidong Ma[a], Yawen Lu[a], Liang Tian[a], Jinyu Zhao[a], Ziang Zhang[a], Yong Zhang[a], Jinduo Zhang[a], Yanxian Ren[a], Haiying Yu[b], Jia Yao[b,*], Dewei Li[c,*], Yanyan Lin[a,*], Wenbo Meng[a,*]

[a]*Department of General Surgery, The First Hospital of Lanzhou University, Lanzhou 730030, China*
[b]*Key Laboratory of Biological Therapy and Regenerative Medicine Transformation of Gansu Province, The First Hospital of Lanzhou University, Lanzhou 730030, China*
[c]*Department of Hepatobiliary Pancreatic Tumor Center, Chongqing University Cancer Hospital, Chongqing 400030, China*

Received 10 April 2025; received in revised form 23 August 2025; accepted 7 November 2025

KEY WORDS

Extrahepatic cholangiocarcinoma;
Primary cells;
Cancer-associated fibroblasts;
Organoids;
Patient-derived xenograft;
HGF;

Abstract Cholangiocarcinoma (CCA) is a markedly desmoplastic tumor, with extrahepatic CCA (eCCA) being the most prevalent subtype. The nonspecific clinical manifestation and early metastatic potential result in a persistently poor overall prognosis. Cancer-associated fibroblasts (CAFs) are one of the major components of the tumor microenvironment implicated in tumor progression and treatment resistance. To faithfully recapitulate the eCCA microenvironment, we established a comprehensive patient-derived preclinical platform comprising CAFs, eCCA primary cells, organoids, and patient-derived xenograft (PDX) models. We found that CAFs facilitated eCCA cell growth, migration, and invasion *in vivo* and *in vitro*. Cytokine profiling revealed that HGF is a key paracrine factor produced by CAFs. CAF-derived HGF activates c-MET signaling to drive gemcitabine resistance in eCCA. Therapeutically, pharmacologic inhibition of c-MET partially resensitized

*Corresponding authors.
E-mail addresses: yaoj06@lzu.edu.cn (Jia Yao), lidewei@cqu.edu.cn (Dewei Li), ldyy_linyy@lzu.edu.cn (Yanyan Lin), mengwb@lzu.edu.cn (Wenbo Meng).
[†]These authors made equal contributions to this work.
Peer review under the responsibility of Chinese Pharmaceutical Association and Institute of Materia Medica, Chinese Academy of Medical Sciences.

https://doi.org/10.1016/j.apsb.2026.02.023

c-MET;
Gemcitabine resistance

eCCA cells to gemcitabine in preclinical models and suppressed tumor progression. In conclusion, our data provides subtype-specific translational evidence that therapeutically targeting the CAF−HGF−c-MET pathway represents a rational strategy to enhance gemcitabine efficacy and improve treatment outcomes in eCCA.

1. Introduction

Cholangiocarcinoma (CCA) is a highly aggressive malignancy originating from the biliary tree[1]. Based on anatomical location, it can be divided into intrahepatic CCA (iCCA) and extrahepatic CCA (eCCA). Additionally, eCCA can be divided into hilar CCA (hCCA) and distal CCA (dCCA)[2]. The incidence and mortality rates of CCA are increasing globally, particularly in Southeast Asia and China, with eCCA accounting for approximately 80% of CCA cases and iCCA accounting for 20%[3-5]. Because of its insidious onset, early lymphatic dissemination, and highly invasive potential, CCA is often diagnosed at an advanced stage, limiting surgical options and resulting in poor prognosis[6]. For patients with unresectable or metastatic disease, gemcitabine combined with cisplatin remains the standard first-line therapy[7]. However, the efficacy of chemotherapy substantially hindered by drug resistance, leading to unsatisfactory survival outcomes[8].

CCA is characterized by its desmoplastic microenvironment, where tumor cells are surrounded by numerous fibroblasts and extracellular matrix[2,9]. Cancer-associated fibroblasts (CAFs) are the predominant cells in the tumor microenvironment (TME)[10]. The best-known marker for CAFs is α-SMA, and other established fibroblast markers include fibroblast activation protein (FAP) and vimentin[11,12]. Previous studies reported that the prevalence of α-SMA-positive CAFs in CCA tissues is associated with tumor progression and poor prognosis[13,14]. Through paracrine secretion of cytokines, growth factors, and extracellular vesicles, CAFs interact with tumor and stromal cells to promote proliferation, invasion[15-17], and therapeutic resistance[18]. Although several CAF-related signaling pathways have been characterized in CCA, the majority of studies have focused on iCCA, leaving the biology and therapeutic vulnerabilities of eCCA largely unexplored.

As a highly heterogeneous tumor, iCCA and eCCA exhibit distinct tumor ecosystems, with significant differences in the composition, diversity, and abundance of various cell types. Embryologically, intrahepatic bile ducts originate from ductal plate cells derived from hepatoblasts during liver development, whereas extrahepatic bile ducts arise from the caudal portion of the ventral foregut endoderm[19]. Recent study has shown that single-cell sequencing of CCA tissues reveals distinct tumor ecosystems between iCCA and eCCA, with significant differences in the composition, diversity, and abundance of various cell types[20]. These developmental distinctions lead to pronounced differences between iCCA and eCCA in molecular signatures, extracellular matrix architecture, and therapeutic responsiveness, thereby warranting subtype-specific translational investigation.

Herein, we sought to elucidate the role of CAFs in driving eCCA progression and therapeutic resistance using a comprehensive patient-derived preclinical platform. We established CAFs, eCCA primary cells, patient-derived organoids (PDOs) model and patient-derived tumor xenograft (PDX) model to faithfully recapitulate the eCCA microenvironment. Through the development of an *in vitro* 3D co-culture model of PDOs and CAFs, we confirmed that CAFs-derived hepatocyte growth factor (HGF) activates the c-MET/PI3K/AKT signaling pathway on eCCA cells, which enhances the malignant phenotype of eCCA cells and induces gemcitabine resistance. Importantly, pharmacologic inhibition of c-MET enhanced gemcitabine therapeutic sensitivity and markedly suppressed tumor growth in PDO and PDX models. While the HGF/c-MET axis has been implicated in other malignancies, our findings provide subtype-specific translational evidence that targeting the CAF−HGF−c-MET signaling pathway represents a rational therapeutic strategy to enhances gemcitabine therapeutic sensitivity in eCCA.

2. Materials and methods

2.1. Clinical sample collection

We obtained fresh eCCA tissues surgically excised from 10 patients with eCCA at the First Hospital of Lanzhou University. Small tissue fragments were randomly excised from each sample and immediately frozen at −80 °C for subsequent DNA extraction. The remaining tissues were utilized for organoids formation and derivation of primary cells. Written informed consents were obtained from each patient. The study was conducted in accordance with the guidelines of the Declaration of Helsinki and approved by the Ethics Committee of the First Hospital of Lanzhou University (Approval number: LDYYLL-2024-773).

2.2. Isolation and construction of eCCA organoids

Fresh tissues were washed twice with cold phosphate-buffered saline (PBS) and subsequently sectioned into approximately 1 mm fragments. Subsequently, the tissues were transferred into advanced DMEM/F-12 (Gibco, USA) supplemented with 200 U collagenase II and digested at 37 °C for 15−30 min. The supernatant was filtered through a 100 μm cell strainer to isolate the cell precipitate. The precipitates were embedded in 50% basement membrane extract (BME, R&D Systems, USA) and incubated at 37 °C for 30 min before the addition of organoid medium. The organoid culture medium contained advanced DMEM/F12 supplemented with 10 mmol/L HEPES, 1 × GlutaMax, 1 × N_2 supplement, 1 × B27 supplement, 50 ng/mL EGF (all from ThermoFisher Scientific, USA), 1.25 mmol/L *N*-acetylcysteine, 5 mmol/L A83-01, 10 nmol/L gastrin I, 500 ng/mL *R*-spondin 1, 10 μmol/L Forskolin and (all from R&D Systems, USA), 1 mmol/L nicotinamide (Sigma−Aldrich, USA) and 100 μg/mL Primocin (InvivoGen, USA). Besides, 10 mmol/L Y-27632

(R&D Systems, USA) was added to the medium for the first three days after seeding or passaging.

2.3. Fibroblast isolation and culture

This was performed as in organoid tissue processing. After tissue digestion and centrifugation, cell precipitates were inoculated into DMEM/F-12 medium supplemented with 10% fetal bovine serum (FBS) and 1% penicillin/streptomycin. Fibroblasts were immortalized through transfection with lentiviruses containing the telomerase reverse transcriptase gene.

2.4. Cell culture

The human primary eCCA cell line CBC3T-1 was isolated as previously described[21]. The human eCCA TFK-1 cell line was procured from Creative Bioarray (NY, USA). All eCCA cell lines were cultured in RPMI 1640 medium supplemented with 10% FBS, 1% penicillin and streptomycin. All cells tested negative for *Mycoplasma* and were cultured in a humidified incubator at 37 °C with 5% CO_2.

For *in vitro* HGF stimulation, the medium was incubated with HGF (R&D Systems, USA) at concentrations of 10 ng/mL. For neutralization experiments, the 5 μg/mL human HGF Antibody (R&D Systems, USA) was used according to the instructions.

2.5. Establishment of drug-resistant CCA cell lines

TFK-1-resistant cell lines were developed using a stepwise increase in concentration method. TFK-1 cells were exposed to 0.1 μmol/L gemcitabine for 48 h and replaced with the normal medium. The drug was reintroduced when the cells returned to normal growth rate, and the concentration was gradually increased. We named the cell line with exponential growth at 5 μmol/L gemcitabine concentration as TFK-1R.

2.6. Whole-exome sequencing (WES) analysis

Samples were sent to Oebiotech (Shanghai, China) for WES analysis. Genomic DNA was extracted from tumors, tumor organoids, and normal adjacent tissues for library preparation utilizing the Agilent SureSelect Human All Exon V6 kit. The qualified sequencing libraries were subjected to sequencing.

Fastp software was used to assess the quality of raw sequencing data and obtain clean reads. Clean reads were compared to the reference genome (GRCh 38.p13) utilizing the Burrows−Wheeler Aligner. Identification of somatic mutations by comparing each cancer sample or tumor organoid with matched normal adjacent tissues. The mutation signature[22] and spectrum of somatic point mutations were analyzed using non-negative matrix factorization. In addition, we used Control-FREEC software to analyze somatic copy number variations (CNV).

2.7. Conditioned medium (CM) collection and cytokine array analysis

CAFs and normal fibroblasts (NFs) were inoculated in 100 mm dishes until 80% fusion; subsequently, they were washed with PBS and cultured in 10 mL serum-free medium for 48 h. The medium was subsequently centrifuged at 1000 × *g* for 5 min at 4 °C to eliminate non-adherent cells and cellular debris. The resultant conditioned medium was named CAF-CM, with NF-CM as a reserve. We followed the operation manual using the Proteome Profiler Human XL Cytokine Array Kit (R&D Systems, USA) to screen for key secreted factors in conditioned medium.

2.8. Enzyme-linked immunosorbent assay (ELISA)

Cells were seeded into six-well plates, grown to 70%−80% confluence, and subsequently cultured in a serum-free medium. The supernatant was obtained after 48 h, and the concentration of HGF was quantified using the Human HGF ELISA Kit (Elabscience, China) according to the manufacturer's instructions.

2.9. Cell counting kit-8 (CCK-8) assay

The eCCA cells were inoculated in 96-well plates (3000 cells/well). After 24 h of incubation, eCCA cells were treated with NF-CM and CAF-CM separately, and cell viability was measured at 0, 24, 48, 72, and 96 h using CCK-8 (APExBIo, USA). For drug sensitivity testing, cells were seeded at 4000 cells/well in 96-well plates and cultured overnight. Cell viability was assessed by treating the cells with different concentrations of gemcitabine, JNJ-38877605 (1 μmol/L), and crizotinib (1 μmol/L) for 48 h. These three drugs were procured from MedChem Express (MCE, USA). Cell survival in both the gemcitabine monotherapy and gemcitabine combined with HGF groups was normalized to the untreated control group without HGF.

2.10. Cell migration and invasion assay

CBC3T-1 cells (5×10^4 cells/well) and TFK-1 (1×10^5 cells/well) cells were seeded in the upper chamber of an 8 μm Transwell insert (Corning, USA) in 24-well plates to assess the migratory capacity of the cells. Additionally, 600 μL of medium containing 15% FBS was added to the lower chamber and incubated in a 5% CO_2 incubator at 37 °C for 48 h. The eCCA cells were inoculated in the upper chamber pre-coated with Matrigel (Matrigel:medium = 1:5, 50 μL/well) to assess the invasive ability. After 48 h of incubation, migrated or invaded cells were fixed with 4% paraformaldehyde and stained with 0.1% crystal violet (Beyotime, China) for 15 min. Three independent replicated experiments were performed.

2.11. 3D co-culture system

Two lentiviral vectors encoding distinct fluorescent proteins—mCherry (red) and Venus (green)—were used to transduce NFs/CAFs and organoids, respectively, to facilitate visualization in the co-culture system. In direct 3D co-culture, the PDOs were digested using TrypLE (Gibco, USA), embedded with CAFs in a 1:2 ratio in 50 μL of BME, and inoculated into 24-well plates coated with 500 μL of organoid medium, allowing direct cell−cell contact. For the Transwell co-culture system, we utilized a 12-well tissue culture insert (Transwell, Corning, USA; pore size 8 μm). Organoids were embedded in 50 μL of BME in the lower chamber. CAFs were inoculated in 200 μL of medium and cultured in this system for 48 h in the upper chamber. For the indirect co-culture system, organoids are embedded in Matrigel droplets and CAFs are seeded in the surrounding matrix area without direct contact, mimicking spatial proximity within the tumor microenvironment. These models were initially tested to evaluate relative HGF secretion capacity, and the direct co-culture

system, which yielded the highest HGF levels, was subsequently selected as the standardized condition for all downstream drug testing assays.

2.12. Drug testing in direct co-culture

The organoid ATP Viability Assay Kit (Absin, China) was utilized to assess organoid viability. PDOs were extracted and enzymatically dissociated into single cells and small cell clusters utilizing TrypLE. PDOs were filtered through a 70 μm mesh to exclude large clusters of organoids. Subsequently, the organoids were resuspended in organoid medium containing 80% BME with CAFs at a ratio of 1:2 and inoculated into clear-bottom 96-well white plates at 8 μL/well. The drugs were added 48 h after plating the organoids. After 72 h of drug incubation, the viability of the co-culture system was detected using the Organoid ATP Viability Assay Kit. A multifunctional microplate reader (BioTek, USA) was used to detect fluorescence.

2.13. Western blotting

Radioimmunoprecipitation assay lysis buffer supplemented with a mixture of protease and phosphatase inhibitors (MCE, USA) was used to extract total cellular protein, which was subsequently analyzed using sodium dodecyl sulfate-polya crylamide gel electrophoresis. Protein supernatants were obtained through centrifugation at 4 °C for bicinchoninic acid protein concentration assessment. Sodium dodecyl sulfate-polyacrylamide gel electrophoresis was subsequently performed. The proteins were transferred to polyvinylidene difluoride membranes (Sigma−Aldrich, USA), blocked with 5% nonfat milk for 1 h, and incubated with primary antibodies overnight at 4 °C. Primary antibody dilution information was as follows: anti-c-MET (1:1000), anti-p-c-MET (1:1000), procured from CST (Boston, USA); anti-p-PI3K (1:1000), anti-PI3K (1:20,000), anti-AKT (1:1000), anti-p-AKT (1:1000), obtained from Abcam (Cambridge, UK); anti-GAPDH (1:5000) procured from Proteintech (IL, USA). The membrane was subsequently incubated with the relevant secondary antibody for 1 h. ChemiScope S6 (Clinx, China) was used to visualize protein bands.

2.14. Hematoxylin and eosin (H&E) and immunohistochemistry (IHC)

The samples were fixed in 4% paraformaldehyde overnight, subsequently embedded in paraffin, and sectioned into 4 μm thick slices. The sections were deparaffinized in xylene, dehydrated through a graded alcohol series, and washed in PBS for H&E staining. For IHC analysis, after the above steps, the sections were heated in a pressure cooker with 10 mmol/L sodium citrate (pH 6.5) for 15 min. Nonspecific antigens were blocked with peroxisomes for 10 min and with 10% normal goat serum for 10 min. Anti-Ki67 (1:1000), CK7 (1:400), and anti-CK19 (1:400, China) were obtained from Maixin Biotechnology (Fuzhou, China). Anti-α-SMA (1:500) and anti-p-c-MET (1:200) was acquired from CST (Boston, USA). Anti-p-PI3K (1:500) was acquired from Abcam (Cambridge, UK). Primary antibodies were incubated at 4 °C overnight. DAB staining was performed after a 30 min incubation with HRP-labeled secondary antibody.

2.15. Immunofluorescence staining

Cells were seeded on polylysine-coated coverslips and fixed with 4% paraformaldehyde for 15 min upon achieving 50% fusion. Cells were subsequently permeabilized with 0.1% Triton X-100 at room temperature for 10 min, blocked with 1% bovine serum albumin for 20 min, and incubated with primary antibody at 4 °C overnight. Primary antibodies α-SMA (1:500), FAP (1:200), and vimentin (1:200) were acquired from CST (Boston, USA). On the subsequent day, the secondary antibody was incubated for 1 h, the nuclei were stained with DAPI, and the images were photographed using an Olympus fluorescence microscope (Olympus Corporation, Japan).

2.16. Multiplexed immunofluorescence staining

Paraffin-embedded eCCA tumor microarrays (TMAs) were procured from Shanghai Outdo Biotechnology (Shanghai, China). They contained 27 cancer tissues and 9 para-tumor tissues. The Opal 4-color Manual IHC Kit was used according to the manufacturer's (PerkinElmer, USA) instructions. The antibody panel included α-SMA (1:300), p-c-MET (1:50), and CK19 (1:400). Pathology analysis software, StrataQuest analysis software (Version 7.1.129, Tissue Gnostic GmbH, Austria) was used for data analysis.

2.17. RNA interference

Specific siRNA sequences targeting MET were obtained from Dona Pharmaceutical Technology Co., Ltd. (Beijing, China). For the siRNA knockdown experiment, target cells were plated in a 6-well plate (1×10^5/well) and cultured for 24 h to reach appropriate confluence. The siRNA transfection complex was then prepared by mixing the specific siRNA with transfection reagent according to the manufacturer's protocol. Following a 5-min incubation at room temperature, the complex was added to the cells. After 24 h of incubation, the transfection medium was replaced with complete growth medium. Cells were harvested 48 h post-transfection for subsequent experimental analyses. The sequences of siRNAs were siRNA-MET1 (5′-UUCAGAAGGUUGCUGAGUATT-3′) and siRNA-MET2 (5′-AGAAUGUCAUUCUACAUGATT-3′).

2.18. Xenograft tumor models

Nonobese diabetic/severe combined immunodeficiency (NOD/SCID) male mice (4−6 weeks old) were procured from GemPharmatech Co., Ltd. (Nanjing, China). Various cells mixed with 50% BME (R&D Systems, USA) were injected subcutaneously into the right subscapular region of NOD/SCID mice (CBC3T-1: CAFs or NFs = 2×10^6:5×10^5 cells/mouse). The tumor size was assessed every 4 days, and mice were euthanized after 40 days. We subcutaneously injected TFK-1 cells combined with 50% BME and CAFs into the flanks of NOD/SCID mice (TFK-1: CAFs = 2×10^6:5×10^5 cells/mouse) to verify the efficacy of the drug on tumors *in vivo*. When the tumor volume reached approximately 150 mm^3 the animals were randomly divided into control, gemcitabine (intraperitoneal injection, 25 mg/kg/4 days), JNJ-38877605 (gavage, 25 mg/kg/day), crizotinib (gavage, 25 mg/kg/day), gemcitabine (intraperitoneal injection, 25 mg/kg/4 days) + JNJ-38877605 (gavage, 25 mg/kg/day), and gemcitabine (intraperitoneal injection, 25 mg/

kg/4 days) + crizotinib (gavage, 25 mg/kg/day) groups. The mice were euthanized after 2 weeks of treatment. Tumors were fixed with 4% paraformaldehyde and subsequently paraffin-embedded for further H&E and IHC.

Surgically resected eCCA tissue was excised into 2 mm diameter sections and implanted subcutaneously into the right subscapular region of NCG mice to construct the PDX model. When the tumor volume exceeded 1000 mm^3, the tumors were passaged in the same way. Stably passaged tumor tissue was subcutaneous implanted into the right subscapular region of NCG mice for drug screening. When the tumor volume attained approximately 150 mm^3, the mice were randomly divided into control, gemcitabine (intraperitoneal injection, 25 mg/kg/4 days), gemcitabine (intraperitoneal injection, 25 mg/kg/4 days) + JNJ-38877605 (gavage, 25 mg/kg/day), and gemcitabine (intraperitoneal injection, 25 mg/kg/4 days) + crizotinib (gavage, 25 mg/kg/day) groups. The mice were euthanized for subsequent analysis after two weeks of drug intervention. We adhered to the ARRIVE guidelines. The animal experiment was performed in accordance with the Guidelines for the Care and Use of Laboratory Animals of China. The Ethics Committee of the First Hospital of Lanzhou University approved the protocol (Approval number: LDYYLL-2024-773).

2.19. Statistical analysis

In vitro experiments were performed independently in triplicate. Data are presented as mean ± standard deviation (SD); GraphPad Prism software (version 8; GraphPad Software, Inc.) was used for data analysis. Comparisons between two groups were evaluated using an unpaired two-tailed Student's *t*-test. For multiple-group comparisons, one-way ANOVA or two-way ANOVA was applied as appropriate. A $P < 0.05$ was considered statistically significant.

3. Results

3.1. Establishment of an eCCA organoid biobank

We established an eCCA organoid biobank, NFs/CAFs, and a primary eCCA cell line (Fig. 1A) to replicate the mutual correlation between CAFs and eCCA *in vitro*. Primary tumor tissues from 10 eCCA cases were used to generate matched PDOs. H&E staining and IHC assay were performed to assess the histological features of eCCA tissue and PDOs (Fig. 1B, Supporting Information Fig. S1). PDOs exhibited atypical cystic and glandular formations, similar to H&E staining of primary tumor tissues, with positive biliary markers cytokeratin 7 (CK7) and cytokeratin 19 (CK19) expression.

WES was used to identify somatic mutations in tumor tissues and organoids. In the eCCA organoid biobank, the total mutation count was consistent except for the tenth case (Supporting Information Fig. S2A). The somatic mutation spectrum and mutation signature of organoids are similar to those of parental tumors (Fig. 1C, Fig. S2B). Furthermore, CNV was conserved in PDOs, and the mean CNV recapitulated the genomic alterations in the parental tumors (Fig. 1D, Fig. S2C). Overall, we have successfully established an eCCA organoid biobank that retains the histological and genetic characteristics of their original tumor tissues.

3.2. CAFs promote the progression of eCCA cells

As important cellular components in the TME, CAFs are essential in CCA occurrence and development. We extracted CAFs and NFs in eCCA tissues and matched adjacent tissues to elucidate the role of CAFs in eCCA progression (Supporting Information Fig. S3A). CAFs are classically fusiform and positive for α-SMA, FAP, and vimentin expression using immunofluorescence (Fig. 2A). Subsequently, we obtained CAF-derived conditioned media (CAF-CM) to culture eCCA cells. Results demonstrated that CAF-CM differentially enhanced the proliferative capacity of TFK-1 and CBC3T-1 cells (Fig. 2B, Fig. S3B). Then, we selected the most proliferative CAF1 and NF1 conditioned media to further assess their impact on eCCA cell metastasis. Our study demonstrated that TFK-1 and CBC3T-1 cells exhibited enhanced motility ability in the presence of CAF-CM or NF-CM, with CAFs exerting a more significant effect on the migration and invasion ability of eCCA cells than NFs (Fig. 2C and D).

Additionally, we assessed the role of CAFs in eCCA progression using PDOs models. We created a 3D co-culture model of PDOs and CAFs and assessed the effect of CAFs on PDOs phenotype. Consistent with previous results, the CAFs co-culture system facilitated an increase in the quantity of organoids compared to PDOs monoculture (Fig. 2E and F). To further confirm the pro-tumorigenic effects of CAFs *in vivo*, we co-injected NFs or CAFs with CBC3T-1 cells into the right scapular region of mice. Notably, the group co-injected with CAFs exhibited the most rapid tumor proliferation compared to the group receiving CBC3T-1 cells alone (Fig. 2G–I). IHC revealed more α-SMA-positive infiltrating fibroblasts in the co-injection group than in the control group, and the expression of Ki67 was significantly upregulated (Fig. 2J). These results illuminated that CAFs promote the malignant phenotype of eCCA cells both *in vitro* and *in vivo.*

3.3. HGF is a key cytokine secreted by CAFs associated with tumor progression

To better understand the paracrine interactions between eCCA cells and CAFs that may influence the malignant phenotype of tumor cells. It was necessary to determine the different cytokine profiles in the culture supernatants of CAFs and NFs cells. Therefore, we performed cytokine array analysis of CAF-CM and NF-CM to identify important secreted factors in CAF-CM that promote eCCA progression. The analysis revealed that the expression levels of HGF, CCL5, angiogenin, and thrombospondin-1 (TSP-1) were significantly higher in CAF-CM compared to NF-CM, with HGF showing the most prominent upregulation (Fig. 3A and B). HGF, a stroma-derived paracrine factor and the exclusive ligand of the c-MET receptor, plays a central role in promoting tumor malignancy, including enhanced proliferative, migration, invasion and chemoresistance[23-25]. We further quantified HGF levels in the conditioned media derived from six paired CAF and NF samples using ELISA. The results confirmed that HGF concentrations were significantly higher in CAF-CM compared to NF-CM, consistent with the findings from the cytokine array analysis (Fig. 3C). Culturing eCCA cells with increasing concentrations of recombinant HGF revealed a dose-dependent enhancement in cell proliferation, indicating that HGF promotes eCCA cell growth in a concentration-dependent manner (Supporting Information Fig. S4A). To validate the role of CAF-derived HGF in promoting eCCA cell proliferation,

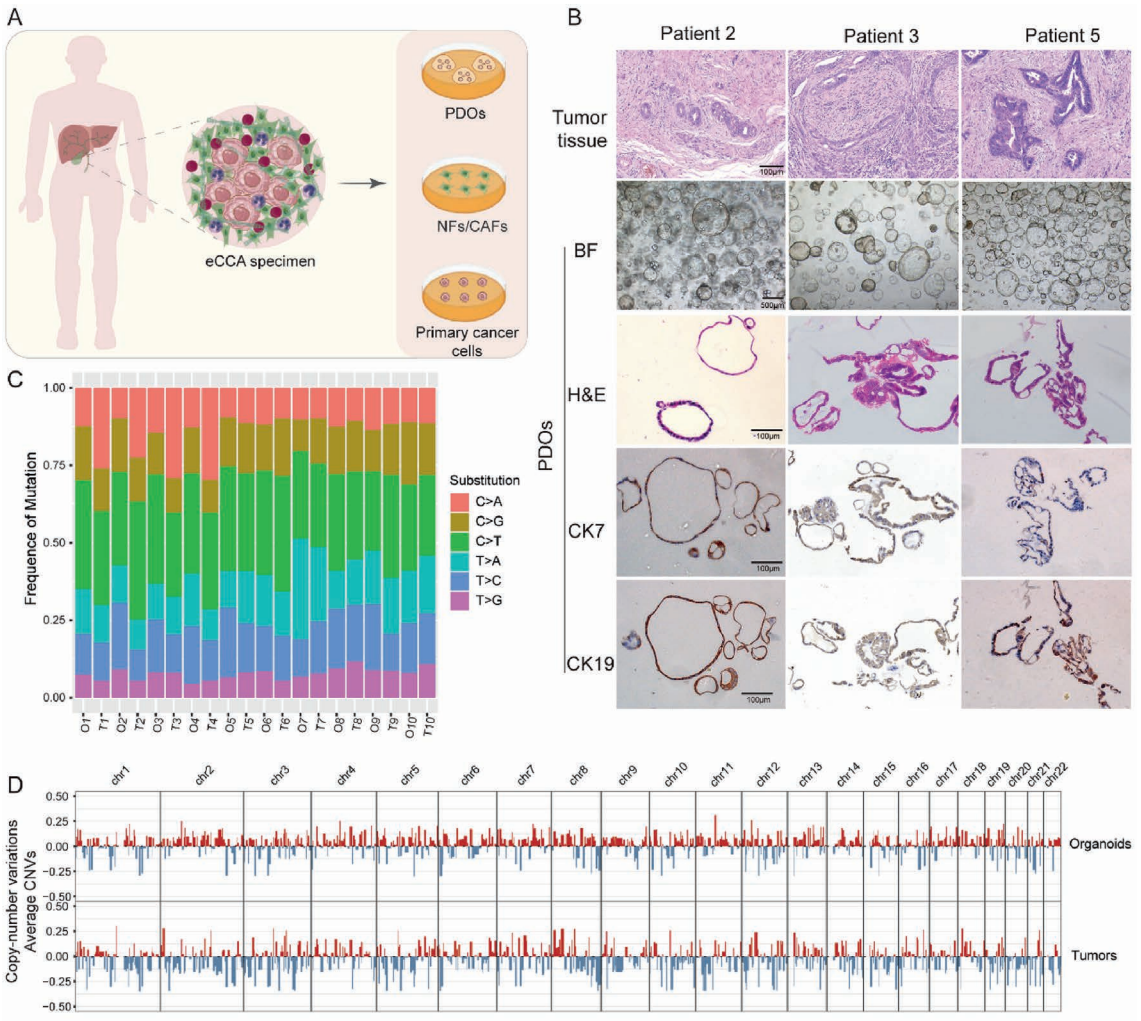

Figure 1 Establishment and genetic characterization of the eCCA organoid biobank. (A) Flowchart for establishing primary cells and PDOs from tumor tissue and para-tumor tissue. (B) Representative H&E staining, IHC and bright field (BF) microscopy images of PDOs and matched tumor tissue (scale bar: 100 μm, scale bar: 500 μm). (C) Analysis of somatic mutation spectrum in tumor tissues (T) and organoids (O). (D) Mean copy-number changes in tumor tissue and organoids.

migration and invasion, eCCA cells were cultured in CAF-CM with or without an HGF-neutralizing antibody. In parallel, cells were treated with recombinant HGF protein as a positive control. The results demonstrated that both CAF-CM and recombinant HGF significantly enhanced the malignant behaviors of eCCA cells, including increased proliferation, migration, and invasion. In contrast, the addition of the HGF-neutralizing antibody markedly suppressed the CAF-CM-induced malignant phenotype (Fig. 3D−F). However, the CCL5 neutralizing antibody and the exogenous addition of CCL5 recombinant protein did not significantly affect eCCA proliferation (Fig. S4B). Angiogenin and TSP-1 were not further investigated due to their relatively low secretion levels in our array analysis. Consequently, we selected HGF as the principal factor for CAF secretion in subsequent studies.

Next, we created eCCA and CAFs co-culture models to better simulate the *in vivo* microenvironment and evaluate the impact of CAFs on PDOs morphology (Fig. 3G). Our analysis of HGF secretion in the co-culture system revealed that CAFs and organoid direct co-culture models produced increased levels of HGF, probably due to the enhanced correlation between each other caused by the 3D direct co-culture, indicating that CAFs are the primary source of HGF (Fig. 3H). Consequently, we used a 3D direct co-culture model of PDOs and CAFs for subsequent studies. In a direct co-culture model of PDOs and CAFs, we observed results consistent with those of previous studies, wherein CAF-derived HGF promoted eCCA organoids proliferation. The addition of an HGF-neutralizing antibody significantly inhibited PDOs proliferation (Fig. 3I). These results demonstrated that CAF-derived HGF is essential in eCCA progression.

3.4. CAF-derived HGF induces eCCA cell progression through activation of the c-MET/PI3K/AKT signaling pathway

The mesenchymal−epithelial transition receptor (MET or c-MET) is a receptor tyrosine kinase, and HGF is a high-affinity ligand for c-MET[26,27]. HGF is predominantly synthesized by stromal and mesenchymal cells, while c-MET receptors are primarily on epithelial cells. The dysregulated phosphorylation activation of the HGF/c-MET axis has been observed in the TME and various

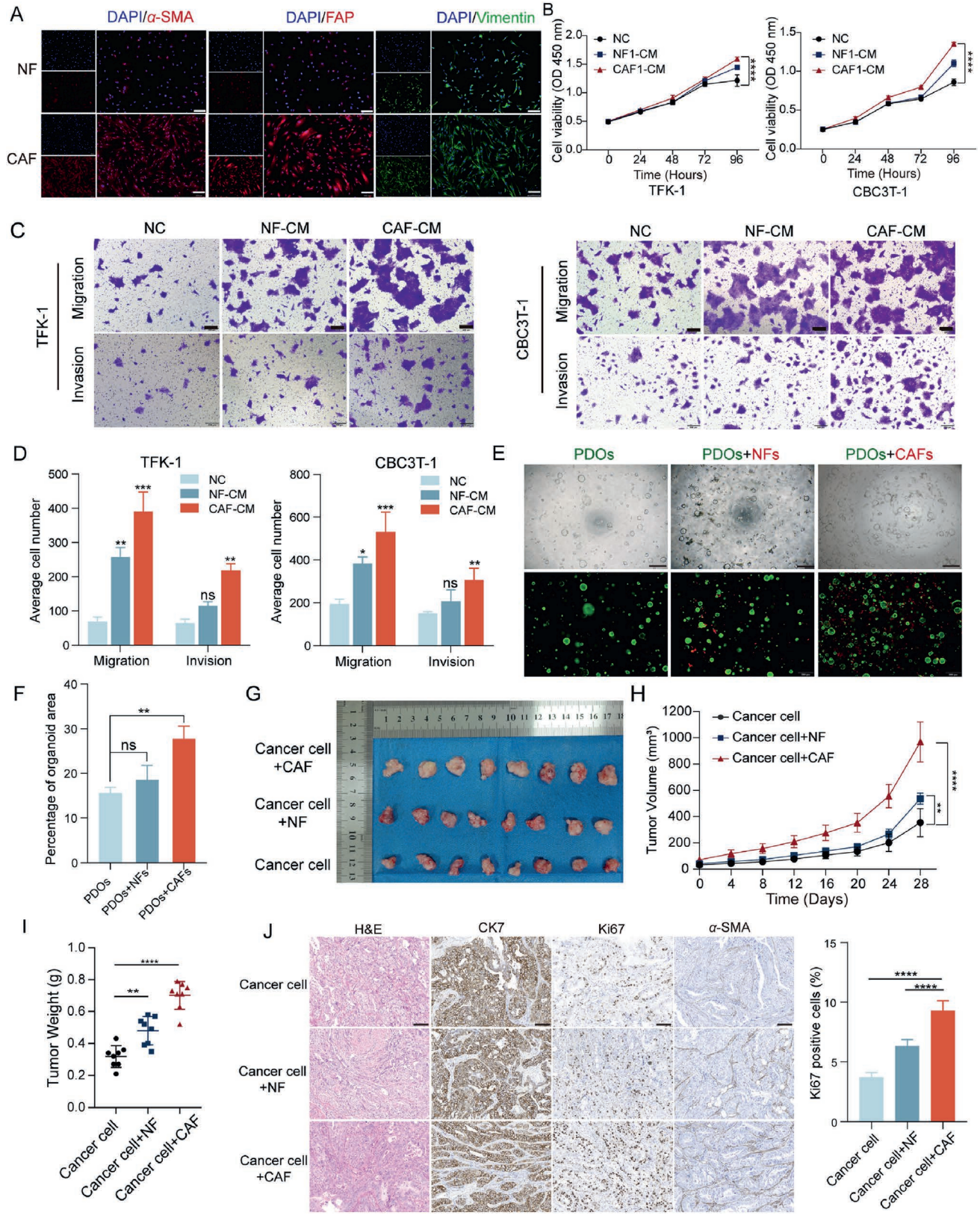

Figure 2 Effect of CAFs on eCCA progression. (A) Immunofluorescence staining of CAFs/NFs showed positive expression of α-SMA, Vimentin and FAP. Scale bar: 200 μm. (B) Effect of CAF-CM/NF-CM on proliferation of TFK-1 and CBC3T-1 cells. Negative control (NC) ($n = 3$). (C, D) Effect of CAF-CM/NF-CM on migration and invasion of TFK-1 and CBC3T-1 cells ($n = 3$). Scale bar: 200 μm. (E, F) Representative fluorescent images of PDOs monocultures or co-cultures with CAFs/NFs and quantitative analysis of total organoid area ($n = 3$). PDOs (green), CAFs/NFs (red). Scale bar: 200 μm. (G) Representative tumor images of cell-derived xenografts: cancer cells, cancer cells + NFs and cancer cells + CAFs. (H, I) Mean tumor volume and tumor weight ($n = 8$). (J) Representative images of H&E and IHC staining of α-SMA, CK7 and Ki67 ($n = 8$). Data are shown as mean ± SD. ns, no significance; $^{*}P < 0.05$; $^{**}P < 0.01$; $^{***}P < 0.001$; $^{****}P < 0.0001$.

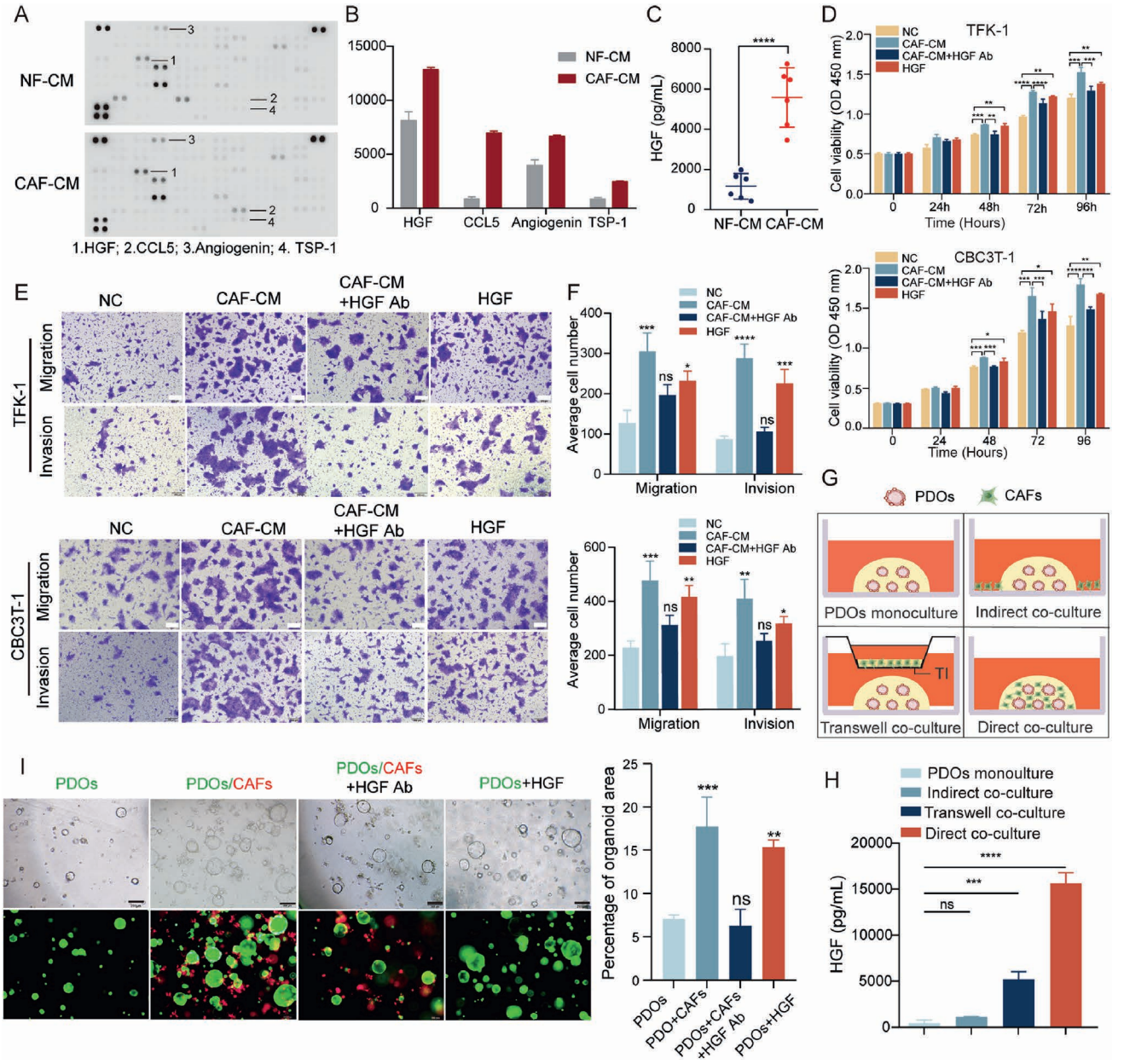

Figure 3 HGF is a key cytokine in CAF-CM affecting eCCA progression. (A, B) Cytokine expression of CAF-CM and NF-CM was detected by cytokine array. HGF, CCL5, Angiogenin and TSP-1 expression was significantly elevated. (C) Levels of HGF in conditioned media from CAFs and NFs derived from six patients with eCCA, measured by ELISA ($n = 6$). (D) Viability of eCCA cells under different treatment conditions—normal control (NC), CAF-CM, CAF-CM with HGF-neutralizing antibody (CAF-CM + HGF Ab), and recombinant HGF (HGF)—measured at 0, 24, 48, 72, and 96 h ($n = 3$). (E, F) Representative images of Transwell assay of eCCA cells treated with CAF-CM or CAF-CM + HGF Ab or HGF for 48 h ($n = 3$). Scale bar: 200 μm. (G, H) Schematic and ELISA-based quantitative analysis of HGF secretion in different co-culture models ($n = 3$): (i) PDO monoculture; (ii) indirect co-culture in which CAFs are seeded in the matrix surrounding PDO-containing Matrigel; (iii) indirect co-culture using a Transwell insert (TI) to allow paracrine interaction without physical contact; (iv) direct co-culture in which PDOs and CAFs are co-embedded in Matrigel to allow cell−cell contact. (I) Representative fluorescence images of organoids in monoculture or direct co-culture with CAFs under different conditions and quantitative analysis of total organoid area ($n = 3$). Scale bar: 200 μm. Data are shown as mean ± SD. ns, no significance; $^{*}P < 0.05$; $^{**}P < 0.01$; $^{***}P < 0.001$; $^{****}P < 0.0001$.

human tumors, including breast, liver, and pancreatic cancers[28]. Overactivation of c-MET is associated with tumor progression and treatment resistance[29,30]. Comparative analysis of c-MET expression in different cells showed that the expression level of eCCA cells was significantly higher compared with that of NFs and CAFs, which further validated that c-MET was highly expressed in tumor cells and lowly expressed in mesenchymal cells (Supporting Information Fig. S5A). In addition, we further validated the expression of c-MET in eCCA tissue microarrays, and the results showed that the expression of c-MET proteins was

more up-regulated in eCCA tissues compared with paraneoplastic tissues (Fig. 4A and B). The heterogeneous expression of c-MET in eCCA provides a molecular basis for HGF-dependent receptor activation. We analyzed the relationship between activated phosphorylated c-MET (p-c-MET) protein levels and α-SMA in eCCA tissue microarrays through multiple immunohistochemical staining techniques (Fig. 4C, Fig. S5B). The results revealed that α-SMA and p-c-MET were highly expressed in cancer, but there was no obvious correlation (Fig. 4D and E, Fig. S5C).

Previous studies reported that the HGF/c-MET signaling pathway activates the downstream PI3K/AKT signaling pathway, promoting tumor growth and drug resistance[31-33]. Furthermore, our previous study showed that PI3K/AKT signaling was significantly increased in CBC3T-1 cells compared to normal bile duct epithelial cells[21]. Hence, we embarked on delineating the effect of HGF on the phosphorylated status of c-MET, PI3K, and AKT in eCCA cell lines. As expected, Western blot analysis revealed a marked increase in the phosphorylation levels of all three proteins following HGF stimulation, indicating that HGF activates the c-MET/PI3K/AKT signaling pathway, indicating that HGF activates the c-MET/PI3K/AKT pathway (Fig. 4F). We next sought to determine whether CAF-secreted HGF was responsible for activating the c-MET/PI3K/AKT signaling pathway in eCCA cells. To this end, eCCA cells were cultured with CAF-CM with or without an HGF-neutralizing antibody. Western blot analysis revealed that CAF-CM induced phosphorylation of c-MET, PI3K, and AKT, whereas the addition of the HGF-neutralizing antibody abolished this activation, confirming that HGF is the principal mediator driving this signaling cascade (Fig. 4G and H). To further validate that this effect is specifically mediated through c-MET activation, we treated eCCA cells with CAF-CM in the presence or absence of the c-MET inhibitors crizotinib and JNJ-38877605. Western blot analysis demonstrated that both inhibitors substantially attenuated CAF-CM-induced phosphorylation of c-MET, PI3K, and AKT, supporting the notion that c-MET is the key upstream effector in this CAF-driven paracrine loop (Fig. 4I and J). Concurrently, functional assays showed that c-MET inhibition significantly suppressed HGF-induced eCCA cell migration and invasion *in vitro* (Fig. S5D). Taken together, these results highlight the central role of CAF-derived HGF in activating the c-MET/PI3K/AKT signaling axis and underscore c-MET as a promising therapeutic target in eCCA.

3.5. Activated HGF/c-MET axis mediates gemcitabine resistance

Previous studies have implicated that the HGF/c-MET signaling pathway in mediating chemoresistance across various tumor types[34,35]. Notably, increased c-MET expression has been associated with reduced gemcitabine sensitivity in pancreatic cancer[36]. Given that gemcitabine remains a standard treatment for eCCA, we hypothesized that c-MET activation may also contribute to drug resistance in this disease. Consistent with this notion, c-MET protein was found to be upregulated in gemcitabine-resistant CCA cell lines and associated with diminished treatment response[37]. To investigate the effect of HGF on gemcitabine sensitivity in eCCA cells, we conducted a CCK-8 assay to evaluate cell viability over time. Cells were treated with gemcitabine in the presence or absence of recombinant HGF, and viability was assessed at 24, 48, 72, and 96 h. The results showed that co-treatment with HGF consistently increased cell viability at each time point compared to gemcitabine treatment alone, indicating that HGF treatment progressively decreased gemcitabine therapeutic sensitivity (Supporting Information Fig. S6A). Dose-response analysis revealed an increase in the IC_{50} of gemcitabine in eCCA cells following HGF exposure, corroborating the chemoresistance phenotype (Fig. 5A). Compared to PDOs monoculture, the three-dimensional co-culture system with CAFs and PDOs further demonstrated that the presence of CAFs enhances tumor resistance to gemcitabine (Fig. 5B). Therefore, we developed a TFK-1 gemcitabine-resistant cell line (TFK-1R) using a stepwise concentration increment method to investigate the effect of the HGF/c-MET signaling pathway on gemcitabine resistance (Fig. 5C). Similarly, compared to parental cells, we observed an upregulation of c-MET protein expression in drug-resistant cells (Fig. 5D), accompanied by stronger activation of c-MET phosphorylation upon HGF stimulation (Fig. S6B). Additionally, cell viability assays showed that the addition of HGF-treated cells reduced the sensitivity of resistant cells to gemcitabine (Fig. 5E). However, under conditions of HGF/c-MET signaling activation, gemcitabine combined with JNJ-38877605 or crizotinib partially reversed this phenotype (Fig. 5F). Consistent with this result, the combination of gemcitabine and c-MET inhibitors enhanced the therapeutic sensitivity of gemcitabine in HGF-stimulated eCCA cells (Fig. 5G). To mechanistically confirm that c-MET silencing attenuates gemcitabine resistance through inhibition of the c-MET/PI3K/AKT axis, we knocked down the *MET* gene using siRNA (Fig. S6C). Western blotting demonstrates that c-MET knockdown in TFK-1R cells diminished phosphorylation-dependent activation of the c-MET/PI3K/AKT pathway (Fig. S6D). Furthermore, genetic inhibition of c-MET attenuated HGF-driven gemcitabine chemoresistance in TFK-1R cells (Fig. S6E). Based on these results, gemcitabine combined with c-MET inhibitors could enhance the therapeutic sensitivity of gemcitabine to eCCA cells.

Meanwhile, we assessed c-MET expression level in 10 organoid cases, and the results revealed varying degrees of c-MET expression in PDOs (Fig. 5H). This indicates that c-MET inhibitors have potential efficacy in eCCA organoids. We subsequently tested the efficacy of gemcitabine alone and in combination with c-MET inhibitors in 3D direct co-culture systems and found that targeting c-MET phosphorylation in the microenvironment increased the sensitivity of gemcitabine treatment (Fig. 5I and J, Supporting Information Fig. S7). Although further studies in immune-competent or longitudinal resistance models are warranted, our findings highlight the HGF/c-MET axis as a relevant therapeutic vulnerability in gemcitabine-resistant eCCA.

3.6. Targeting CAF-activated c-MET phosphorylation in vivo enhances the therapeutic sensitivity of eCCA to gemcitabine

Subsequently, we examined the *in vivo* therapeutic effects of c-MET inhibitors combined with gemcitabine in eCCA. CAFs and eCCA cells were co-injected into the right subscapular region of NOD/SCID mice. After the tumor volume grew to approximately 150 mm^3, gemcitabine, JNJ-38877605, crizotinib, and gemcitabine combined with c-MET inhibitors were administered, respectively (Fig. 6A). After two weeks of drug treatment, we found that gemcitabine combined with the c-MET inhibitor group significantly reduced the tumor size. Treatment with gemcitabine alone or c-MET inhibitor alone was also effective; however, the combination inhibitor group was more effective, evidenced by the smaller macroscopic tumor size (Fig. 6B), a slower tumor growth rate and diminished tumor weight (Fig. 6C and D). IHC staining revealed that c-MET inhibitor reduced the

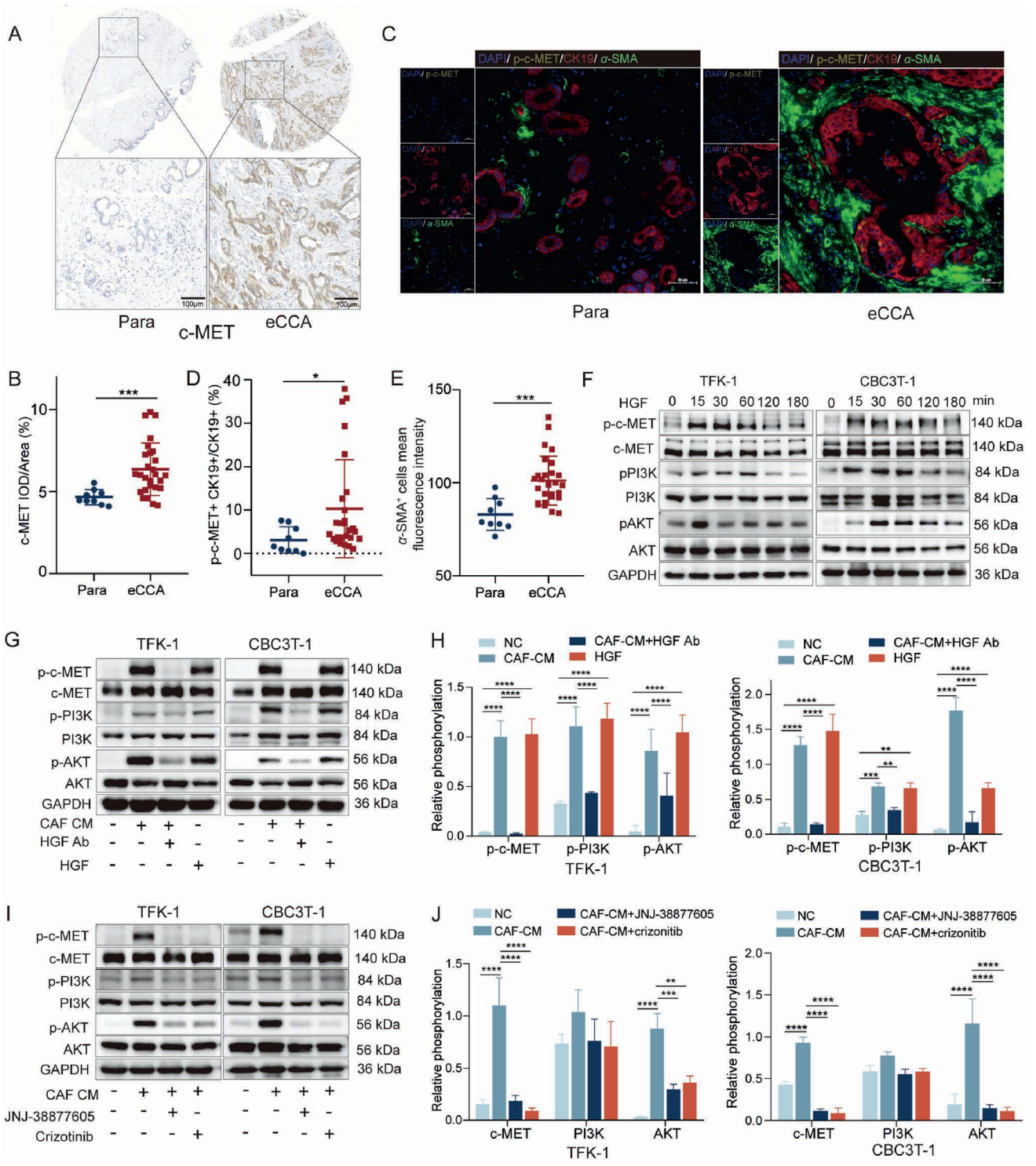

Figure 4 Inhibition of HGF/c-MET signaling pathway suppresses CAFs-induced eCCA progression. (A) Representative IHC images of c-MET expression in eCCA ($n = 27$) and para-tumor tissues ($n = 9$). (B) IHC staining intensity of c-MET in eCCA tissues ($n = 27$) and para-tumor tissues ($n = 9$) of TMAs. (C) Representative images of multiplex immunofluorescence staining (α-SMA, green; p-c-MET, yellow; CK19, red) in eCCA and para-tumor tissue. (D) Percentage of p-c-MET^{+}CK19^{+} cells to CK19^{+} cells in eCCA tissues and para-tumor tissues. (E) Mean fluorescence intensity of α-SMA^{+} in eCCA and para-tumor tissues. (F) Western blot analysis of p-c-MET, total c-MET, p-PI3K, total PI3K, *p*-AKT, and total AKT in TFK-1 and CBC3T-1 cells treated with recombinant HGF at different time points (15, 30, 60, 120 min). (G, H) Western blotting of the c-MET/PI3K/AKT signaling pathway in TFK-1 and CBC3T-1 cells under the following conditions: normal control (NC), CAF-CM, CAF-CM supplemented with an HGF-neutralizing antibody (CAF-CM + HGF Ab), or recombinant HGF ($n = 3$). (I, J) Western blot analysis of c-MET/PI3K/AKT pathway activity in eCCA cells treated with CAF-CM, with or without the c-MET inhibitors JNJ-38877605 or crizotinib ($n = 3$). Data are shown as mean ± SD. *$P < 0.05$; **$P < 0.01$; ***$P < 0.001$; ****$P < 0.0001$.

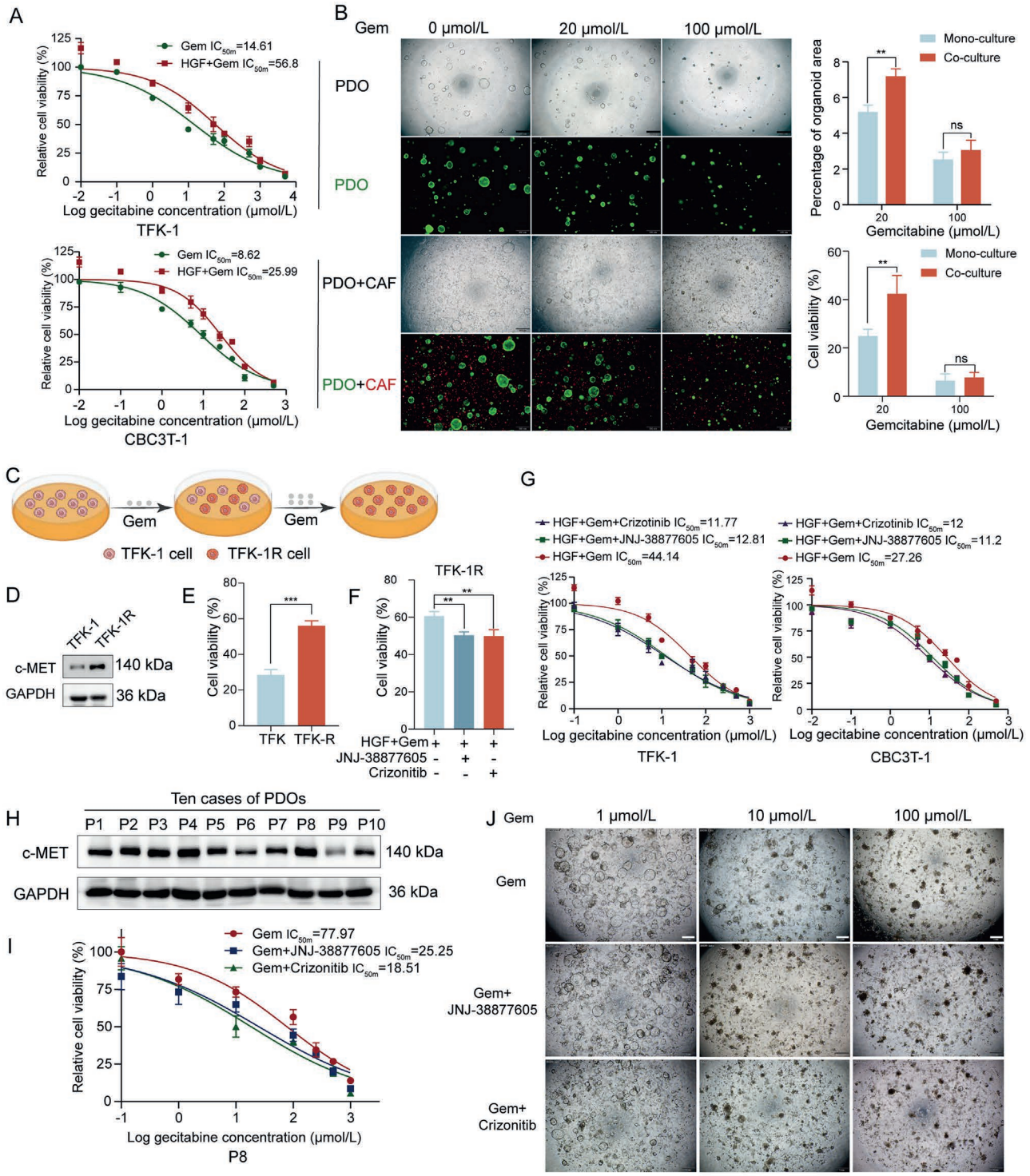

Figure 5 Targeting the HGF/c-MET signaling pathway enhances gemcitabine treatment sensitivity *in vitro*. (A) Cell viability of TFK-1 and CBC3T-1 cells treated with gemcitabine or gemcitabine combined with HGF ($n = 3$). (B) Representative images of the sensitivity of gemcitabine to PDOs monoculture systems or direct co-culture systems with CAFs ($n = 3$). PDOs (green), CAFs (red). The percentage of total area of the PDOs was quantified and the viability was determined. Scale bar: 500 μm. (C) Schematic diagram for the construction of TFK-1 gemcitabine-resistant cells (TFK-1R). (D) Western blot analysis of c-MET protein levels in parental TFK-1 cells and gemcitabine-resistant TFK-1 cells (TFK-1R). (E) Cell viability of 100 μmol/L gemcitabine-treated TFK-1 and TFK-1R cells ($n = 3$). (F) Cell viability of TFK-1R cells treated with 100 μmol/L gemcitabine or in combination with c-MET inhibitor under conditions of added HGF ($n = 3$). (G) Dose−response curves of gemcitabine alone or in combination with c-MET inhibitors for treatment of TFK-1 and CBC3T-1 cells under conditions of added HGF ($n = 3$). (H) Western blot analysis of c-MET protein levels in PDOs established from 10 cases of eCCA. (I, J) Representative images and dose−response curves of gemcitabine alone or in combination with c-MET inhibitor in a direct co-culture system of PDOs and CAFs. Patient 8 (P8) ($n = 3$). Scale bar: 500 μm. Data are shown as mean ± SD. ns, no significance; $^{**}P < 0.01$; $^{***}P < 0.001$.

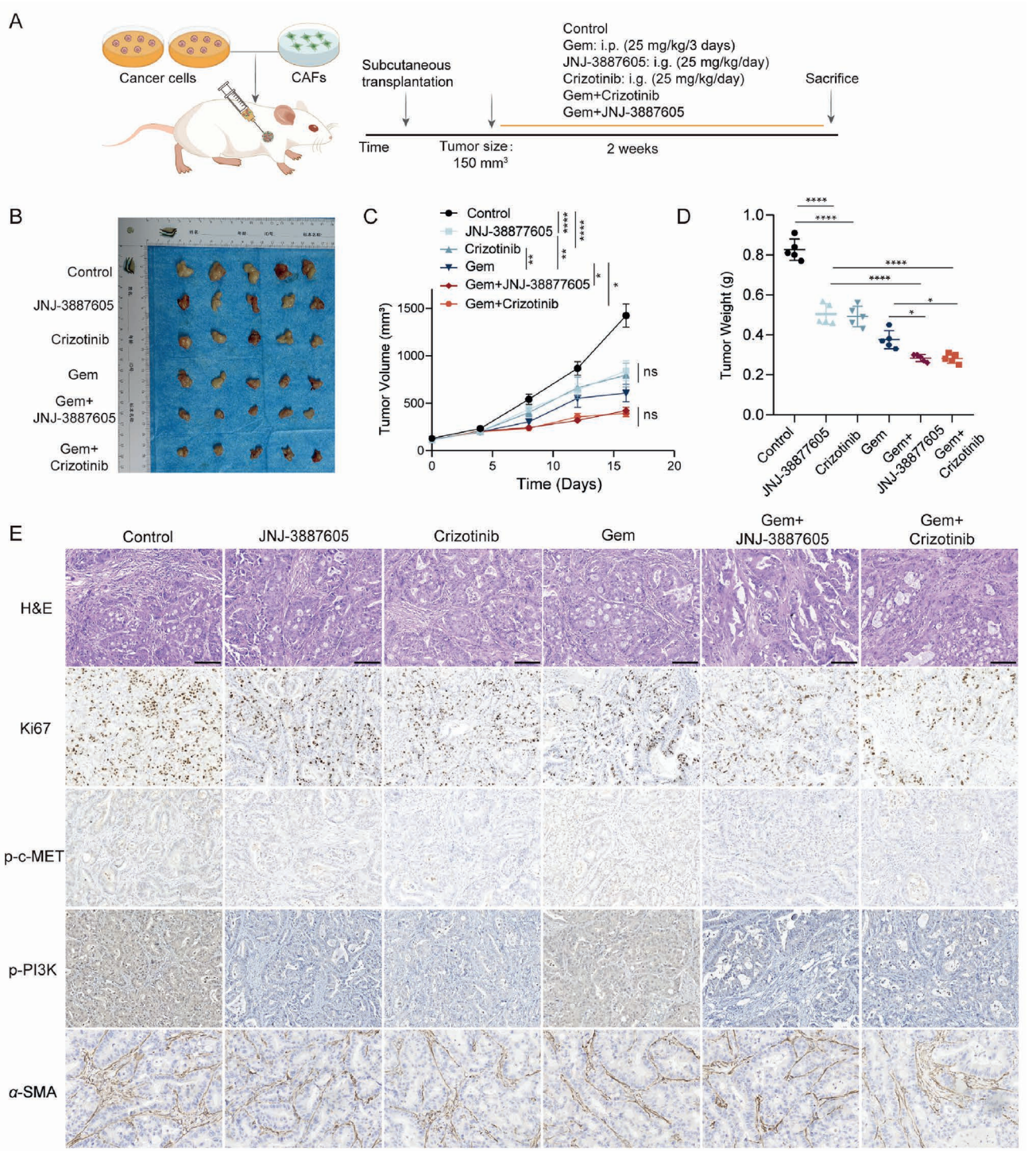

Figure 6 The combination of gemcitabine and c-MET inhibitors reduced cell-derived xenotransplantation growth. (A) Schematic diagram of the process of co-injection of cancer cells and CAFs into mice subcutaneously. (B−D) Representative tumor images of cell-derived xenografts treated with gemcitabine, c-MET inhibitors, or gemcitabine combined with c-MET inhibitor. Tumor volume and mass were calculated ($n = 5$). (E) H&E and IHC staining were used to assess the expression of Ki67, p-c-MET, p-PI3K and α-SMA in subcutaneous tumor tissues of mice. i.p., intraperitoneal injection; i.g., intragastric. Scale bar, 100 μm. Data are shown as mean ± SD. ns, no significance; $^{*}P < 0.05$; $^{**}P < 0.01$; $^{****}P < 0.0001$.

c-MET phosphorylation level. Compared to gemcitabine monotherapy, gemcitabine combination therapy reduced Ki67 expression and inhibited the activation of the c-MET/PI3K/AKT signaling pathway (Fig. 6E).

The PDX model partially preserves tumor stromal cells, such as CAFs and vascular endothelial cells, which closely resemble those in the original donor tumors in terms of histological expression and biological behavior[38,39]. This feature

renders the PDX model particularly suitable for investigating tumor−microenvironment interactions. Consequently, we further evaluated the efficacy of the combination of c-MET inhibitor and gemcitabine with eCCA PDX models (Fig. 7A). Consistent with our previous data, while gemcitabine monotherapy has an inhibitory effect on tumor growth, combination therapy results in significant tumor regression (Fig. 7B−D). IHC of Ki67, p-c-MET and p-PI3K further confirmed that combination therapy significantly reduced tumor proliferation and c-MET/PI3K/AKT signaling activation. Although c-MET inhibition significantly suppressed tumor growth and enhanced gemcitabine sensitivity, our α-SMA IHC analyses indicated that the CAF population remained largely unaffected post-treatment (Fig. 7E). This suggests that the observed therapeutic benefit results primarily from disruption of CAF-derived paracrine signaling, rather than depletion of CAFs themselves. In general, these findings reveal that targeting CAF-activated HGF/c-MET signaling inhibits eCCA cell growth *in vivo* and enhances gemcitabine drug sensitivity.

4. Discussion

CAFs alter TME by secreting cytokines, exosomes, and metabolites, thereby facilitating tumor proliferation, drug resistance, and metastasis, affecting tumor prognosis[40]. Although the crosstalk between CAFs and surrounding cells has been extensively studied, the precise mechanisms by which CAFs regulate tumor cell

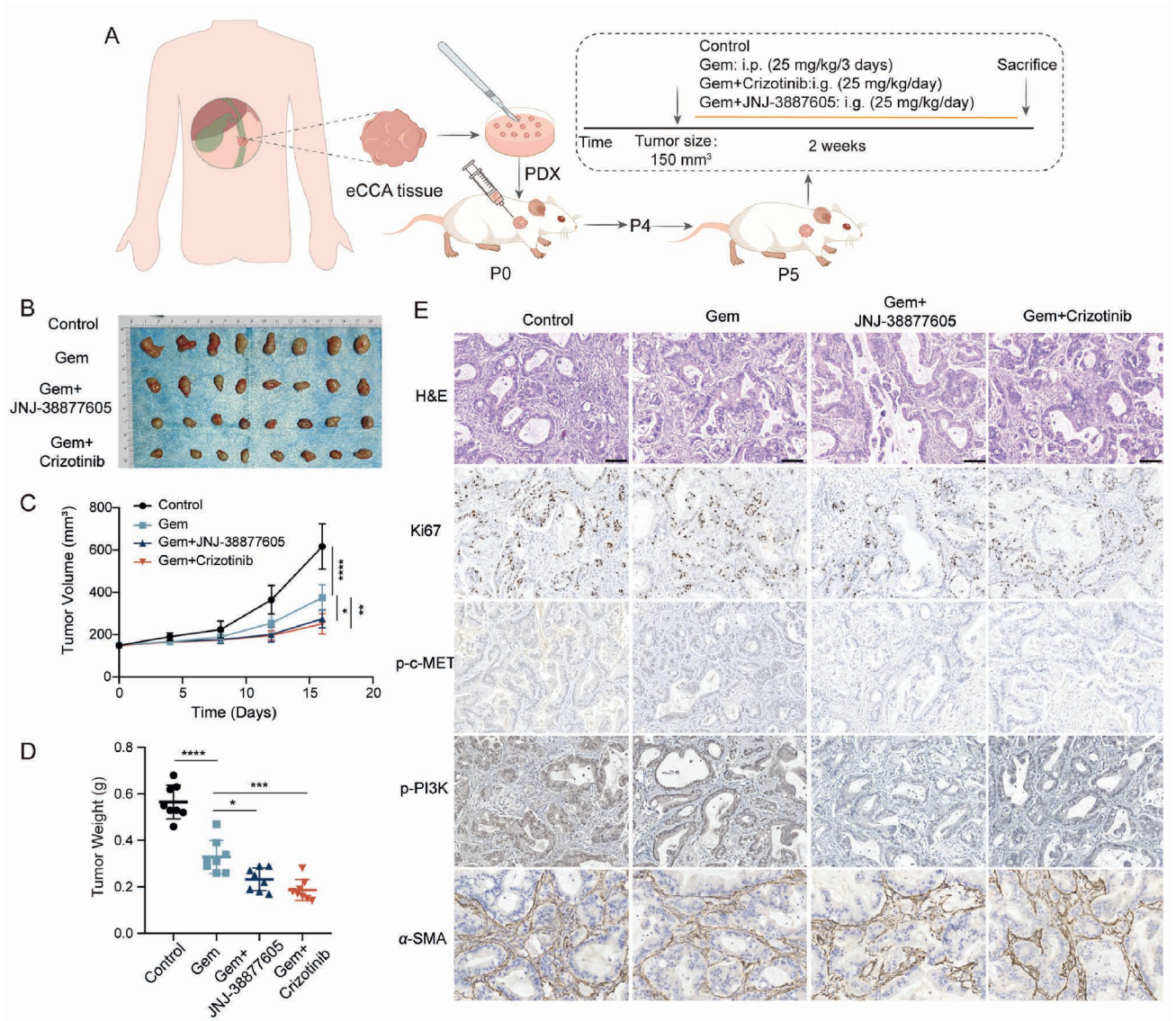

Figure 7 The combination of gemcitabine and c-MET inhibitors reduced PDX tumor growth. (A) Schematic diagram of the PDX model construction process used for screening drugs. Passage 0 (P0), passage 4 (P4), passage 5 (P5). (B) Representative tumor images of PDX treated with gemcitabine alone or gemcitabine in combination with c-MET inhibitors. (C, D) Tumor volume and mass statistics ($n = 8$). (E) H&E and IHC staining were used to assess the expression of Ki67, p-c-MET, p-PI3K and α-SMA in PDX tissues. Scale bar, 100 μm. Data are expressed as mean ± SD. *$P < 0.05$; **$P < 0.01$; ****$P < 0.0001$.

behavior remain incompletely understood, especially in eCCA. In this study, we provide subtype-specific translational evidence that the CAF-activated HGF/c-MET axis contributes to gemcitabine resistance in eCCA and represents a rational therapeutic target.

To elucidate the role of CAFs in eCCA progression, we established a comprehensive patient-derived preclinical platform encompassing NFs/CAFs, eCCA primary cells, PDOs and PDX model. The reliability of the organoid biobank was verified through WES and the expression of biliary lineage markers. Using this system, CAFs significantly enhanced eCCA cell proliferation, migration, and invasion *in vitro* and *in vivo*. Cytokine profiling identified HGF as a major CAF-secreted mediator that activates c-MET signaling in eCCA. Direct CAF−tumor contact within 3D co-culture models further amplified HGF secretion, likely through adhesion molecule engagement and juxtacrine signaling. In contrast, indirect or Transwell co-culture models permitted only paracrine interactions, resulting in lower HGF levels. These findings collectively underscore the importance of CAF−tumor spatial interactions in modulating HGF production within the eCCA microenvironment.

Neutralization experiments confirmed that HGF is the dominant factor mediating CAF-induced c-MET activation. The c-MET protein, encoded by the *MET* proto-oncogene, functions as the specific receptor for HGF. Upon HGF binding, c-MET undergoes phosphorylation and triggers multiple downstream oncogenic cascades, including the PI3K/AKT pathway, which collectively regulate tumor cell proliferation, survival, invasion, epithelial−mesenchymal transition, and therapeutic resistance[25,41]. Aberrant activation of the HGF/c-MET signaling axis can arise from *MET* amplification, mutation, or overexpression of either HGF or c-MET. In the present study, we focused on a distinct mechanism—paracrine hyperactivation of c-MET signaling driven by excessive HGF secretion from CAFs. Consistent with this, c-MET was highly expressed in eCCA tissues, and multiplex immunofluorescence revealed marked phosphorylation of c-MET in tumor cells. Notably, this activation did not correlate linearly with CAF marker expression, suggesting that additional stromal populations, such as tumor-associated macrophages and endothelial cells, may also contribute to HGF secretion within the tumor microenvironment[42]. Thus, while CAFs are a major contributor, they are not the sole source of HGF[43]. Moreover, c-MET activation exhibits a threshold phenomenon, wherein even low concentrations of HGF can achieve maximal receptor phosphorylation. Therefore, further increases in CAF abundance may not necessarily enhance c-MET activation.

Given the established role of the HGF/c-MET pathway in multiple malignancies[44,45], we next evaluated c-MET inhibition in our eCCA models. As expected, pharmacologic blockade of c-MET effectively attenuated CAF-induced activation of the c-MET/PI3K/AKT cascade and significantly reduced the migratory and invasive capacities of eCCA cells. Although targeted therapies against HGF/c-MET have demonstrated clinical benefits in certain tumor types, single-agent c-MET inhibition has shown limited efficacy in most cancers, likely due to compensatory signaling and microenvironmental resistance[46,47]. Because of existing chemoresistance mechanisms, gemcitabine is ineffective as a first-line treatment for advanced CCA. In our study, CAF-derived HGF was identified as a major stromal driver of gemcitabine resistance, while pharmacologic inhibition of c-MET partially resensitized eCCA models to gemcitabine in preclinical settings. Consistent with this observation, c-MET expression was elevated in gemcitabine-resistant cell lines, and pharmacologic inhibition of c-MET enhances gemcitabine sensitivity in TFK-1R resistant cells. Across ten PDO cases, heterogeneous c-MET expression levels were observed. Nonetheless, the combination of gemcitabine with a c-MET phosphorylation inhibitor achieved a better therapeutic effect in 3D direct co-culture systems of PDOs and CAFs. This enhanced therapeutic response was further validated in both cell line-derived xenografts and PDX models. To investigate the interactions between CAFs and cancer cells in a controlled environment without interference from the immune system, we employed NOD/SCID mice for subcutaneous co-transplantation experiments involving different cells, and NCG mice for establishing PDX models. While the immunodeficient status of these mice may not fully recapitulate the complex tumor−immune system interactions observed in human patients, it was a necessary choice to ensure successful tumor engraftment and to focus on the specific mechanisms of CAF-mediated HGF/c-MET signaling in eCCA. Nevertheless, the absence of longitudinal resistance evolution and immune-competent systems remains a limitation. Future studies incorporating long-term treatment models and immune-competent settings are warranted to fully understand the therapeutic impact of targeting the CAF−c-MET axis.

Although the CAF−HGF−c-MET signaling axis has been reported in several malignancies, including iCCA, its role in eCCA remains poorly characterized. Notably, eCCA differs from iCCA in terms of epidemiology, anatomical features, treatment strategies, and prognosis. While iCCA incidence has been rising globally, eCCA still represents the predominant subtype in East Asia and often presents with obstructive jaundice and complex biliary involvement, leading to greater surgical challenges and poorer treatment outcomes. The limitation of this study is that the small tissue sample size of eCCA did not yield sufficient clinical prognostic data for further analysis. Additionally, it has been reported that c-MET overexpression contributes to gemcitabine resistance in pancreatic cancer. Targeting c-MET can effectively inhibit pancreatic cancer tumor growth; however, its mechanism requires further investigation[48,49]. To date, the precise mechanism underlying c-MET protein overexpression and its association with gemcitabine resistance in eCCA remains unclear. Future research will focus on clarifying the mechanism of c-MET activation in gemcitabine-resistant eCCA and the development of precision-targeted drugs against drug resistance mechanisms. Moreover, Future studies incorporating immune-competent models, longitudinal treatment designs, and single-cell or spatial transcriptomic profiling will be essential to define CAF heterogeneity and its therapeutic implications.

5. Conclusions

CAFs-derived HGF in TME promotes eCCA progression and contributes to gemcitabine resistance by activating the c-MET/PI3K/AKT signaling pathway. Targeted inhibition of the HGF/c-MET signaling pathway partially resensitized eCCA models to gemcitabine and suppressed tumor growth in preclinical modes. Our study provides subtype-specific translational evidence supporting a therapeutic strategy that combines c-MET inhibition with gemcitabine to mitigate stromal-driven resistance in eCCA. Collectively, these findings underscore the importance of tumor−stroma interactions in shaping therapeutic response and highlight the CAF−HGF−c-MET axis as a viable target for improving clinical outcomes in this challenging malignancy.

Acknowledgments

This study was supported by the National Natural Science Foundation of China (82060551), Scientific Research Program of

Health Industry in Gansu Province (GSWSKY2020-11, China), the National Natural Science Foundation of China (32160230), Special Projects for Scientific and Technological Achievements and Applications of Gansu Province (24ZDCA008, China), Science and Technology Bureau Talent Innovation Program of Lanzhou Chengguan District (2022RCCX0024, China).

Author contributions

Mingzhen Bai: Writing − Original Draft, Conceptualization, Methodology, Investigation. Ping Yue: Conceptualization, Methodology, Investigation. Wenkang Fu: Conceptualization, Methodology, Investigation. Ruyang Zhong: Methodology, Investigation, Data Curation. Chongfei Huang: Methodology, Investigation. Ningzu Jiang: Methodology, Investigation. Long Gao: Methodology, Investigation. Ningning Mi: Formal analysis. Haidong Ma: Methodology, Investigation. Yawen Lu: Investigation. Liang Tian: Formal analysis. Jinyu Zhao: Investigation. Yong Zhang: Validation. Jinduo Zhang: Data Curation. Yanxian Ren: Investigation. Haiying Yu: Methodology. Jia Yao: Writing − Review & Editing, Project administration, Funding acquisition. Dewei Li: Writing − Review & Editing, Project administration. Yanyan Lin: Writing − Review & Editing, Project administration. Wenbo Meng: Writing − Review & Editing, Supervision, Project administration, Funding acquisition.

Conflicts of interest

The authors declare no conflicts of interest.

Appendix A. Supporting information

Supporting information to this article can be found online at https://doi.org/10.1016/j.apsb.2026.02.023.

References

1. Razumilava N, Gores GJ. Cholangiocarcinoma. *Lancet* 2014;**383**:2168−79.
2. Brindley PJ, Bachini M, Ilyas SI, Khan SA, Loukas A, Sirica AE, et al. Cholangiocarcinoma. *Nat Rev Dis Primers* 2021;**7**:65.
3. DeOliveira ML, Cunningham SC, Cameron JL, Kamangar F, Winter JM, Lillemoe KD, et al. Cholangiocarcinoma−thirty-one-year experience with 564 patients at a single institution. *Ann Surg* 2007;**245**:755−62.
4. Banales JM, Marin JJG, Lamarca A, Rodrigues PM, Khan SA, Roberts LR, et al. Cholangiocarcinoma 2020: the next horizon in mechanisms and management. *Nat Rev Gastroenterol Hepatol* 2020;**17**:557−88.
5. Banales JM, Cardinale V, Carpino G, Marzioni M, Andersen JB, Invernizzi P, et al. Expert consensus document: cholangiocarcinoma: current knowledge and future perspectives consensus statement from the European network for the study of cholangiocarcinoma (ENS-CCA). *Nat Rev Gastroenterol Hepatol* 2016;**13**:261−80.
6. Goeppert B, Frauenschuh L, Zucknick M, Stenzinger A, Andrulis M, Klauschen F, et al. Prognostic impact of tumour-infiltrating immune cells on biliary tract cancer. *Br J Cancer* 2013;**109**:2665−74.
7. Valle JW, Furuse J, Jitlal M, Beare S, Mizuno N, Wasan H, et al. Cisplatin and gemcitabine for advanced biliary tract cancer: a meta-analysis of two randomised trials. *Ann Oncol* 2014;**25**:391−8.
8. Marin JJG, Lozano E, Herraez E, Asensio M, Di Giacomo S, Romero MR, et al. Chemoresistance and chemosensitization in cholangiocarcinoma. *Biochim Biophys Acta Mol Basis Dis* 2018;**1864**:1444−53.
9. Brivio S, Cadamuro M, Strazzabosco M, Fabris L. Tumor reactive stroma in cholangiocarcinoma: the fuel behind cancer aggressiveness. *World J Hepatol* 2017;**9**:455−68.
10. Vaquero J, Aoudjehane L, Fouassier L. Cancer-associated fibroblasts in cholangiocarcinoma. *Curr Opin Gastroenterol* 2020;**36**:63−9.
11. Affo S, Nair A, Brundu F, Ravichandra A, Bhattacharjee S, Matsuda M, et al. Promotion of cholangiocarcinoma growth by diverse cancer-associated fibroblast subpopulations. *Cancer Cell* 2021;**39**:866−82.e11.
12. Kalluri R. The biology and function of fibroblasts in cancer. *Nat Rev Cancer* 2016;**16**:582−98.
13. Chuaysri C, Thuwajit P, Paupairoj A, Chau-In S, Suthiphongchai T, Thuwajit C. α-Smooth muscle actin-positive fibroblasts promote biliary cell proliferation and correlate with poor survival in cholangiocarcinoma. *Oncol Rep* 2009;**21**:957−69.
14. Zhang XF, Dong M, Pan YH, Chen JN, Huang XQ, Jin Y, et al. Expression pattern of cancer-associated fibroblast and its clinical relevance in intrahepatic cholangiocarcinoma. *Hum Pathol* 2017;**65**:92−100.
15. Claperon A, Mergey M, Aoudjehane L, Ho-Bouldoires THN, Wendum D, Prignon A, et al. Hepatic myofibroblasts promote the progression of human cholangiocarcinoma through activation of epidermal growth factor receptor. *Hepatology* 2013;**58**:2001−11.
16. Okabe H, Beppu T, Ueda M, Hayashi H, Ishiko T, Masuda T, et al. Identification of CXCL5/ENA-78 as a factor involved in the interaction between cholangiocarcinoma cells and cancer-associated fibroblasts. *Int J Cancer* 2012;**131**:2234−41.
17. Qin XL, Lu M, Li G, Zhou YJ, Liu ZY. Downregulation of tumor-derived exosomal miR-34c induces cancer-associated fibroblast activation to promote cholangiocarcinoma progress. *Cancer Cell Int* 2021;**21**:373.
18. Vaquero J, Lobe C, Tahraoui S, Clapéron A, Mergey M, Merabtene F, et al. The IGF2/IR/IGF1R pathway in tumor cells and myofibroblasts mediates resistance to EGFR inhibition in cholangiocarcinoma. *Clin Cancer Res* 2018;**24**:4282−96.
19. Strazzabosco M, Fabris L. Development of the bile ducts: essentials for the clinical hepatologist. *J Hepatol* 2012;**56**:1159−70.
20. Liu C, Wang X, Liu E, Zong Y, Yu W, Jiang Y, et al. Deciphering cholangiocarcinoma heterogeneity and specific progenitor cell niche of extrahepatic cholangiocarcinoma at single-cell resolution. *J Hematol Oncol* 2025;**18**:66.
21. Bai M, Jiang N, Fu W, Huang C, Tian L, Mi N, et al. Establishment and characterization of a novel hilar cholangiocarcinoma cell line, CBC3T-1. *Hum Cell* 2024;**37**:364−75.
22. Alexandrov LB, Nik-Zainal S, Wedge DC, Aparicio SA, Behjati S, Biankin AV, et al. Signatures of mutational processes in human cancer. *Nature* 2013;**500**:415−21.
23. Shi X, Wang M, Zhang Y, Guo X, Liu M, Zhou Z, et al. Hypoxia activated HGF expression in pancreatic stellate cells confers resistance of pancreatic cancer cells to EGFR inhibition. *EBioMedicine* 2022;**86**:104352.
24. Xia Y, Huang C, Zhong M, Zhong H, Ruan R, Xiong J, et al. Targeting HGF/c-met signaling to regulate the tumor microenvironment: implications for counteracting tumor immune evasion. *Cell Commun Signal* 2025;**23**:46.
25. Fu J, Su X, Li Z, Deng L, Liu X, Feng X, et al. HGF/c-met pathway in cancer: from molecular characterization to clinical evidence. *Oncogene* 2021;**40**:4625−51.
26. Bottaro DP, Rubin JS, Faletto DL, Chan AM, Kmiecik TE, Vande Woude GF, et al. Identification of the hepatocyte growth factor receptor as the c-Met proto-oncogene product. *Science* 1991;**251**:802−4.
27. Uchikawa E, Chen Z, Xiao GY, Zhang X, Bai XC. Structural basis of the activation of c-Met receptor. *Nat Commun* 2021;**12**:4074.
28. Mohan CD, Shanmugam MK, Gowda SGS, Chinnathambi A, Rangappa KS, Sethi G. c-Met pathway in human malignancies and its targeting by natural compounds for cancer therapy. *Phytomedicine* 2024;**128**:155379.

29. Organ SL, Tsao MS. An overview of the c-Met signaling pathway. *Ther Adv Med Oncol* 2011;**3**:S7−19.
30. Parizadeh SM, Jafarzadeh-Esfehani R, Fazilat-Panah D, Hassanian SM, Shahidsales S, Khazaei M, et al. The potential therapeutic and prognostic impacts of the c-Met/HGF signaling pathway in colorectal cancer. *IUBMB Life* 2019;**71**:802−11.
31. Yang MH, Baek SH, Um JY, Ahn KS. Anti-neoplastic effect of ginkgolide C through modulating c-Met phosphorylation in hepatocellular carcinoma cells. *Int J Mol Sci* 2020;**21**:8303.
32. Ding X, Xi W, Ji J, Cai Q, Jiang J, Shi M, et al. HGF derived from cancer-associated fibroblasts promotes vascularization in gastric cancer *via* PI3K/AKT and ERK1/2 signaling. *Oncol Rep* 2018;**40**: 1185−95.
33. Wang B, Liu W, Liu C, Du K, Guo Z, Zhang G, et al. Cancer-associated fibroblasts promote radioresistance of breast cancer cells *via* the HGF/c-Met signaling pathway. *Int J Radiat Oncol Biol Phys* 2023; **116**:640−54.
34. Peng H, Xue R, Ju Z, Qiu J, Wang J, Yan W, et al. Cancer-associated fibroblasts enhance the chemoresistance of $CD73^{+}$ hepatocellular carcinoma cancer cells *via* HGF−MET−ERK1/2 pathway. *Ann Transl Med* 2020;**8**:856.
35. Singh S, Lamichhane A, Rafsanjani Nejad P, Heiss J, Baumann H, Gudneppanavar R, et al. Therapeutic targeting of stromal-tumor HGF−MET signaling in an organotypic triple-negative breast tumor model. *Mol Cancer Res* 2022;**20**:1166−77.
36. Hage C, Rausch V, Giese N, Giese T, Schönsiegel F, Labsch S, et al. The novel c-Met inhibitor cabozantinib overcomes gemcitabine resistance and stem cell signaling in pancreatic cancer. *Cell Death Dis* 2013;**4**:e627.
37. Kerdkumthong K, Roytrakul S, Songsurin K, Pratummanee K, Runsaeng P, Obchoei S. Proteomics and bioinformatics identify drug-resistant-related genes with prognostic potential in cholangiocarcinoma. *Biomolecules* 2024;**14**:969.
38. Hidalgo M, Amant F, Biankin AV, Budinska E, Byrne AT, Caldas C, et al. Patient-derived xenograft models: an emerging platform for translational cancer research. *Cancer Discov* 2014;**4**:998−1013.
39. Tentler JJ, Tan AC, Weekes CD, Jimeno A, Leong S, Pitts TM, et al. Patient-derived tumour xenografts as models for oncology drug development. *Nat Rev Clin Oncol* 2012;**9**:338−50.
40. Chen Y, McAndrews KM, Kalluri R. Clinical and therapeutic relevance of cancer-associated fibroblasts. *Nat Rev Clin Oncol* 2021;**18**: 792−804.
41. Gherardi E, Birchmeier W, Birchmeier C, Vande Woude G. Targeting met in cancer: rationale and progress. *Nat Rev Cancer* 2012;**12**: 89−103.
42. Piao Y, Park SY, Henry V, Smith BD, Tiao N, Flynn DL, et al. Novel MET/TIE2/VEGFR2 inhibitor altiratinib inhibits tumor growth and invasiveness in bevacizumab-resistant glioblastoma mouse models. *Neuro Oncol* 2016;**18**:1230−41.
43. De Silva DM, Roy A, Kato T, Cecchi F, Lee YH, Matsumoto K, et al. Targeting the hepatocyte growth factor/MET pathway in cancer. *Biochem Soc Trans* 2017;**45**:855−70.
44. Recondo G, Che J, Janne PA, Awad MM. Targeting met dysregulation in cancer. *Cancer Discov* 2020;**10**:922−34.
45. Min W, Wang Y, Shen H, Zheng M, Tong C, Shen H, et al. Discovery of potent and selective c-Met inhibitors for met-amplified hepatocellular carcinoma treatment. *Eur J Med Chem* 2024;**264**: 116025.
46. Bouattour M, Raymond E, Qin SK, Cheng AL, Stammberger U, Locatelli G, et al. Recent developments of c-Met as a therapeutic target in hepatocellular carcinoma. *Hepatology* 2018;**67**: 1132−49.
47. Huang L, Xie K, Li H, Wang R, Xu X, Chen K, et al. Suppression of c-Met-overexpressing tumors by a novel c-Met/CD3 bispecific antibody. *Drug Des Dev Ther* 2020;**14**:3201−14.
48. Brandes F, Schmidt K, Wagner C, Redekopf J, Schlitt HJ, Geissler EK, et al. Targeting cMET with INC280 impairs tumour growth and improves efficacy of gemcitabine in a pancreatic cancer model. *BMC Cancer* 2015;**15**:71.
49. Shah AN, Summy JM, Zhang J, Park SI, Parikh NU, Gallick GE. Development and characterization of gemcitabine-resistant pancreatic tumor cells. *Ann Surg Oncol* 2007;**14**:3629−37.